

# Structured Binary Neural Networks for Image Recognition

Bohan Zhuang, Chunhua Shen, Mingkui Tan, Lingqiao Liu, and Ian Reid

**Abstract**—In this paper, we propose methods to train convolutional neural networks (CNNs) with both binarized weights and activations, leading to quantized models that are specifically friendly to mobile devices with limited power capacity and computation resources. Previous works on quantizing CNNs often seek to approximate the floating-point information using a set of discrete values, which we call value approximation, typically assuming the same architecture as the full-precision networks. Here we take a novel “structure approximation” view of quantization—it is very likely that different architectures designed for low-bit networks may be better for achieving good performance. In particular, we propose a “network decomposition” strategy, termed Group-Net, in which we divide the network into groups. Thus, each full-precision group can be effectively reconstructed by aggregating a set of homogeneous binary branches. In addition, we learn effective connections among groups to improve the representation capability. Moreover, the proposed Group-Net shows strong generalization to other tasks. For instance, we extend Group-Net for accurate semantic segmentation by embedding rich context into the binary structure. Furthermore, for the first time, we apply binary neural networks to object detection. Experiments on both classification, semantic segmentation and object detection tasks demonstrate the superior performance of the proposed methods over various quantized networks in the literature. Our methods outperform the previous best binary neural networks in terms of accuracy and computation efficiency.

**Index Terms**—Binary neural networks, quantization, image classification, semantic segmentation, object detection.

## CONTENTS

|          |   |   |                   |  |    |
|----------|---|---|-------------------|--|----|
| <b>1</b> | <b>Introduction</b>                               | 2 | 5.2.1             | Layer-wise vs. group-wise binary decomposition . . . . . | 9  |
| <b>2</b> | <b>Related Work</b>                               | 3 | 5.2.2             | Effect of the soft gate . . . . .                        | 9  |
| <b>3</b> | <b>Method</b>                                     | 4 | 5.2.3             | Effect of the number of bases . . . . .                  | 9  |
| 3.1      | Problem definition . . . . .                      | 4 | 5.2.4             | Effect of the group space . . . . .                      | 10 |
| 3.2      | Structured Binary Network Decomposition . . . . . | 4 | 5.3               | Evaluation on semantic segmentation . . . . .            | 10 |
| 3.2.1    | Layer-wise binary decomposition . . . . .         | 4 | 5.3.1             | Experiments on FCN . . . . .                             | 10 |
| 3.2.2    | Group-wise binary decomposition . . . . .         | 5 | 5.3.2             | Experiments on DeepLabv3 . . . . .                       | 11 |
| 3.2.3    | Learning for decomposition . . . . .              | 6 | 5.4               | Evaluation on object detection . . . . .                 | 12 |
| 3.3      | Extension to semantic segmentation . . . . .      | 6 | 5.4.1             | Performance evaluation . . . . .                         | 12 |
| 3.4      | Extension to object detection . . . . .           | 7 | 5.4.2             | Detection components analysis                            | 12 |
| <b>4</b> | <b>Discussions</b>                                | 7 | <b>6</b>          | <b>Conclusion</b>  | 12 |
| <b>5</b> | <b>Experiment</b>                                 | 8 | <b>References</b> |  | 13 |
| 5.1      | Evaluation on ImageNet . . . . .                  | 8 |                   |  |    |
| 5.1.1    | Implementation details . . . . .                  | 8 |                   |  |    |
| 5.1.2    | Comparison with binary neural networks . . . . .  | 8 |                   |  |    |
| 5.1.3    | Comparison with fix-point approaches . . . . .    | 9 |                   |  |    |
| 5.2      | Ablation study on ImageNet classification         | 9 |                   |  |    |

- *B. Zhuang, C. Shen, L. Liu and I. Reid are with Australian Centre for Robotic Vision, The University of Adelaide, Australia. E-mail: (first-name.lastname@adelaide.edu.au). C. Shen is the corresponding author.*
- *M. Tan is with South China University of Technology, China. E-mail: (tanmingkui@scut.edu.cn).*

## 1 INTRODUCTION

Designing deeper and wider convolutional neural networks has led to significant breakthroughs in many machine learning tasks, such as image classification [1], [2], object segmentation [3], [4] and object detection [5], [6]. However, accurate deep models often require billions of FLOPs, which makes it infeasible for deep models to run many real-time applications on resource constrained mobile platforms. To solve this problem, many existing works focus on network pruning [7], [8], [9], low-bit quantization [10], [11] and/or efficient architecture design [12], [13]. Among them, the quantization approaches represent weights and activations with low bitwidth fixed-point integers, and thus the dot product can be computed by several XNOR-popcount bit-wise operations. The XNOR of two bits requires only a single logic gate instead of using hundreds units for floating point multiplication [14], [15]. Binarization [16], [17] is an extreme quantization approach where both the weights and activations are represented by a single bit, either +1 or -1. In this paper, we aim to design highly accurate binary neural networks (BNNs) from both the quantization and efficient architecture design perspectives.

Existing quantization methods can be mainly divided into two categories. The first category methods seek to design more effective optimization algorithms to find better local minima for quantized weights. These works either introduce knowledge distillation [10], [18], [19] or use loss-aware objectives [20], [21]. The second category approaches focus on improving the quantization function [22], [23], [24]. To maintain good performance, it is essential to learn suitable mappings between discrete values and their floating-point counterparts. However, designing quantization function is highly non-trivial especially for BNNs, since the quantization functions are often non-differentiable and gradients can only be roughly approximated.

The above two categories of methods belong to *value approximation*, which seeks to quantize weights and/or activations by preserving most of the representational ability of the original network. However, the value approximation approaches have a natural limitation that it is merely a local approximation. Moreover, these methods often lack of adaptive ability to general tasks. Given a pretrained model on a specific task, the quantization error will inevitably occur and the final performance may be affected.

In this paper, we seek to explore a third category called *structure approximation*. The main objective is to redesign a binary architecture that can directly match the capability of a floating-point model. In particular, we propose a Structured Binary Neural Network called Group-Net to partition the full-precision model into groups and use a set of parallel binary bases to approximate its floating-point structure counterpart. In this way, higher-level structural information can be better preserved than the *value approximation* approaches.

Furthermore, relying on the proposed structured model, we are able to design flexible binary structures according to different tasks and exploit task-specific information or structures to compensate the quantization loss and facilitate training. For example, when transferring Group-Net from image classification to semantic segmentation, we are motivated by the structure of Atrous Spatial Pyramid Pooling

(ASPP) [25]. In DeepLab v3 [26] and v3+ [4], ASPP is merely applied on the top of extracted features while each block in the backbone network can employ one atrous rate only. In contrast, we propose to directly apply different atrous rates on parallel binary bases in the backbone network, which is equivalent to absorbing ASPP into the feature extraction stage. Thus, we significantly boost the performance on semantic segmentation, without increasing the computation complexity of the binary convolutions.

In general, it is nontrivial to extend previous *value approximation* based quantization approaches to more challenging tasks such as semantic segmentation (or other general computer vision tasks). However, as will be shown, our Group-Net can be easily extended to other tasks. Nevertheless, it is worth mentioning that value and structure approximation are complementary rather than contradictory. In other words, both are important and should be exploited to obtain highly accurate BNNs.

To improve the balance between accuracy and complexity, several works [27], [28], [29], [30], [31] propose to employ a linear combination of binary tensors to approximate the filters and/or activations while still possessing the advantage of binary operations. In particular, Guo *et al.* [27] recursively performs residual quantization on pretrained full-precision weights and does convolution on each binary weight base. Similarly, Li *et al.* [28] propose to expand the input feature maps into binary bases in the same manner. And Lin *et al.* [29] further expand both weights and activations with a simple linear approach. Our methods are also motivated by those energy-efficient architecture design approaches [12], [13], [32], [33] which seek to replace the traditional expensive convolution with computational efficient convolutional operations (i.e., depthwise separable convolution,  $1 \times 1$  convolution). Nevertheless, we propose to design binary network architectures for dedicated hardware from the quantization view. We highlight that while most existing quantization works focus on directly quantizing the full-precision architecture, at this point in time we do begin to explore alternative architectures that shall be better suited for dealing with binary weights and activations. In particular, apart from decomposing each group into several binary bases, we also propose to learn the connections between each group by introducing a fusion gate. Moreover, Group-Net can be possibly further improved with Neural Architecture Search methods [34], [35], [36].

Our contributions are summarized as follows:

- We propose to design accurate BNNs structures from the *structure approximation* perspective. Specifically, we divide the networks into groups and approximate each group using a set of binary bases. We also propose to automatically learn the decomposition by introducing soft connections.
- The proposed Group-Net has strong flexibility and can be easily extended to tasks other than image classification. For instance, in this paper we propose Binary Parallel Atrous Convolution (BPAC), which embeds rich multi-scale context into BNNs for accurate semantic segmentation. Group-Net with BPAC significantly improves the performance while maintaining the complexity compared to employ Group-

Net only.

- To the best of our knowledge, we are the first to apply binary neural networks on general semantic segmentation and object detection tasks.
- We evaluate our models on ImageNet, PASCAL VOC and COCO datasets based on ResNet. Extensive experiments show the proposed Group-Net achieves the state-of-the-art trade-off between accuracy and computational complexity.

This paper extends our preliminary results, which appeared in [37], in several aspects. 1) In addition to the image classification and semantic segmentation task, we further generalize Group-Net to object detection. As a result, we apply binary neural networks on the three fundamental computer vision tasks. 2) For image classification, we conduct more ablation study and more comprehensive analysis. 3) For semantic segmentation, we also implement on DeepLabv3 and provide useful instructions. We have also provided more technical details here.

## 2 RELATED WORK

**Network quantization:** The recent increasing demand for implementing fixed point deep neural networks on embedded devices motivates the study of low-bit network quantization. Quantization based methods represent the network weights and/or activations with very low precision such as 1 bit, 2 bits or 4 bits, thus yielding highly compact DNN models compared to their floating-point counterparts. BNNs [16], [17] propose to constrain both weights and activations to binary values (i.e., +1 and -1), where the multiplication-accumulations can be replaced by purely  $\text{xnor}(\cdot)$  and  $\text{popcount}(\cdot)$  operations, which are in general much faster. However, BNNs still suffer from significant accuracy decrease compared with the full precision counterparts. To narrow this accuracy gap, ternary networks [38], [39] and even higher bit fixed-point quantization [22] methods are proposed. In general, quantization approaches target at tackling two main problems. On one hand, some works target at designing more accurate quantizer to minimize information loss. For the uniform quantizer, works in [40], [41] explicitly parameterize and optimize the upper and/or lower bound of the activation and weights. To reduce the quantization error, non-uniform approaches are proposed to better approximate the data distribution. In particular, authors of [42] propose to explicitly minimize the cross entropy between the full-precision distribution and the discrete categorical distribution. LQ-net [24] proposes to jointly optimize the quantizer and the network parameters, where it provides a closed-form solution and solves the quantization basis iteratively during the training. On the other hand, because of the non-differentiable quantizer, some literature focuses on relaxing the discrete optimization problem. A typical approach is to train with regularization [43], [44], where the optimization problem becomes continuous while gradually adjusting the data distribution towards quantization levels. Moreover, Hou *et al.* [20], [21] propose the loss-aware quantization by directly optimizing the discrete objective function. Apart from the two challenges, with the popularization of neural architecture search (NAS), Wang

*et al.* [45] further propose to employ reinforcement learning to automatically determine the bit-width of each layer without human heuristics. Unlike the previous local tensor approximation approaches, we directly design BNNs from a structure approximation perspective and show strong generalization on a few mainstream computer vision tasks.

**Efficient architecture design:** There has been a rising interest in designing efficient architecture recently. Efficient model designs like GoogLeNet [46] and SqueezeNet [32] propose to replace  $3 \times 3$  convolutional kernels with  $1 \times 1$  size to reduce the complexity while increasing the depth and accuracy. Additionally, separable convolutions are also proved to be effective in Inception approaches [47], [48]. This idea is further generalized as depthwise separable convolutions as in Xception [12], MobileNet [13], [49] and ShuffleNet [33] to obtain energy-efficient network structure. To avoid handcrafted heuristics to explore the enormous design space, NAS [34], [35], [36], [50], [51] has been explored for automatically sample the design space and improve the model quality.

**Semantic segmentation:** Deep learning based semantic segmentation is popularized by the Fully Convolutional Networks (FCNs) [3]. Recent prominent direction have emerged: using the encoder-encoder structure [4], [52]; relying on dilated convolutions to keep the reception fields without downsampling the spatial resolution too much [26], [53]; employing multi-scale feature fusion [25], [54]; employing probabilistic graphical models [55], [56].

However, these approaches typically focus on designing complex modules for improving accuracy while sacrificing the inference efficiency to some extent. To make semantic segmentation applicable, several methods have been proposed to design real-time semantic segmentation models. Recently, works of [57], [58] apply neural architecture search for exploring more accurate model with less Multi-Adds operations. Yu *et al.* [59] propose BiSeNet, where a spatial path extracts high-resolution features and a context path obtains sufficient receptive fields to achieve high speed and accuracy. ESPNet [53], [60] design efficient spatial pyramid for real-time semantic segmentation under resource constraints. In contrast, we instead propose to accelerate semantic segmentation frameworks from the quantization perspective, which is parallel to the above approaches. Given a pretrained full-precision model, we can replace multiply-accumulations by the XNOR-popcount operations, which would bring great benefits for ARM and FPGA platforms. We may be the first to apply binary neural networks on semantic segmentation and achieve promising results.

**Object detection:** Object detection has shown great success with deep neural networks. As one of the dominant detection framework, two-stage detection methods [6], [61], [62] first generate region proposals and then refine them by subsequent networks. The dominant method Faster-RCNN [6] first proposes an end-to-end detection framework by introducing a region proposal network (RPN). Another main category is the one-stage methods which are represented by YOLO [5], [63], [64] and SSD [65]. The objective is to improve the detection efficiency by directly classifying and regressing the pre-defined anchors without the proposal generation step. RetinaNet [66] proposes a novel focal loss to tackle the extreme foreground-background class imbalance

encountered during training in one-stage detectors.

Two recent developing trends in object detection that are worth to mention. On the one hand, designing light-weight detection frameworks is crucial since mobile applications usually require real-time, low-power and fully embeddable. For example, the work of [67] and [68] propose to train a tiny model by distilling knowledge from a deeper teacher network. MNasNet [69] proposes to automatically search for mobile CNNs which achieve better mAP quality than MobileNets for COCO object detection. On the other hand, anchor-free detection [70], [71] is now gaining more and more attention. Since detection becomes proposal free and anchor free, it can avoid the hyperparameters and complicated computation related to anchor boxes. Moreover, Tian *et al.* [70] propose a simple fully convolutional anchor-free one-stage detector that achieves comparable performance with the anchor-based one-stage detectors. In this paper, we explore to unify these two cutting-edge trends by proposing to binarize the one-stage anchor-free detection framework. Note that, we are the first to train a binary object detection model in the literature.

### 3 METHOD

Most previous methods in the literature have focused on value approximation by designing accurate binarization functions for weights and activations (e.g., multiple binarizations [27], [28], [29], [30], [31]). In this paper, we seek to binarize both weights and activations of CNNs from a “structure approximation” view. In the following, we first define the research problem and present some basic knowledge about binarization in Sec. 3.1. Then, in Sec. 3.2, we explain our binary architecture design strategy. Finally, in Sec. 3.3 and Sec. 3.4, we describe how to use task-specific attributes to generalize our approach to semantic segmentation and object detection, respectively.

#### 3.1 Problem definition

For a convolutional layer, we define the input  $\mathbf{x} \in \mathbb{R}^{c_{in} \times w_{in} \times h_{in}}$ , weight filter  $\mathbf{w} \in \mathbb{R}^{c \times w \times h}$  and the output  $\mathbf{y} \in \mathbb{R}^{c_{out} \times w_{out} \times h_{out}}$ , respectively.

**Binarization of weights:** Following [17], we approximate the floating-point weight  $\mathbf{w}$  by a binary weight filter  $\mathbf{b}^w$  and a scaling factor  $\alpha \in \mathbb{R}^+$  such that  $\mathbf{w} \approx \alpha \mathbf{b}^w$ , where  $\mathbf{b}^w$  is the sign of  $\mathbf{w}$  and  $\alpha$  calculates the mean of absolute values of  $\mathbf{w}$ . In general,  $\text{sign}(\cdot)$  is non-differentiable and so we adopt the straight-through estimator [72] (STE) to approximate the gradient calculation. Formally, the forward and backward processes can be given as follows:

$$\begin{aligned} \text{Forward : } \mathbf{b}^w &= \text{sign}(\mathbf{w}), \\ \text{Backward : } \frac{\partial \ell}{\partial \mathbf{w}} &= \frac{\partial \ell}{\partial \mathbf{b}^w} \cdot \frac{\partial \mathbf{b}^w}{\partial \mathbf{w}} \approx \frac{\partial \ell}{\partial \mathbf{b}^w}, \end{aligned} \quad (1)$$

where  $\ell$  is the loss.

**Binarization of activations:** For activation binarization, we utilize the piecewise polynomial function to approximate

the sign function as in [73]. The forward and backward can be written as:

$$\begin{aligned} \text{Forward : } b^a &= \text{sign}(x), \\ \text{Backward : } \frac{\partial \ell}{\partial x} &= \frac{\partial \ell}{\partial b^a} \cdot \frac{\partial b^a}{\partial x}, \\ \text{where } \frac{\partial b^a}{\partial x} &= \begin{cases} 2 + 2x : -1 \leq x < 0 \\ 2 - 2x : 0 \leq x < 1 \\ 0 : \text{otherwise} \end{cases} \end{aligned} \quad (2)$$

#### 3.2 Structured Binary Network Decomposition

In this paper, we seek to design a new structural representation of a network for quantization. First of all, note that a float number in computer is represented by a fixed-number of binary digits. Motivated by this, rather than directly doing the quantization via “value decomposition”, we propose to decompose a network into binary structures while preserving its representability.

Specifically, given a floating-point residual network  $\Phi$  with  $N$  blocks, we decompose  $\Phi$  into  $P$  binary fragments  $[\mathcal{F}_1, \dots, \mathcal{F}_P]$ , where  $\mathcal{F}_i(\cdot)$  can be any binary structure. Note that each  $\mathcal{F}_i(\cdot)$  can be different. A natural question arises: can we find some simple methods to decompose the network with binary structures so that the representability can be exactly preserved? To answer this question, we here explore two kinds of architectures for  $\mathcal{F}(\cdot)$ , namely layer-wise decomposition and group-wise decomposition in Sec. 3.2.1 and Sec. 3.2.2, respectively. Then we present a novel strategy for automatic decomposition in Sec. 3.2.3.

##### 3.2.1 Layer-wise binary decomposition

The key challenge of binary decomposition is how to reconstruct or approximate the floating-point structure. The simplest way is to approximate in a layer-wise manner. Let  $B(\cdot)$  be a binary convolutional layer and  $\mathbf{b}_i^w$  be the binarized weights for the  $i$ -th base. In Fig. 1 (c), we illustrate the layer-wise feature reconstruction for a single block. Specifically, for each layer, we aim to fit the full-precision structure using a set of binarized homogeneous branches  $\mathcal{F}(\cdot)$  given a floating-point input tensor  $\mathbf{x}$ :

$$\mathcal{F}(\mathbf{x}) = \frac{1}{K} \sum_{i=1}^K B_i(\mathbf{x}) = \frac{1}{K} \sum_{i=1}^K (\mathbf{b}_i^w \oplus \text{sign}(\mathbf{x})), \quad (3)$$

where  $\oplus$  is bitwise operations  $\text{xnor}(\cdot)$  and  $\text{popcount}(\cdot)$ ,  $K$  is the number of branches. During the training, the structure is fixed and each binary convolutional kernel  $\mathbf{b}_i^w$  is directly updated with end-to-end optimization. The scale scalar can be absorbed into batch normalization when doing inference. Note that all  $B_i$ ’s in Eq. (3) have the same topology as the original floating-point counterpart. Each binary branch gives a rough approximation and all the approximations are aggregated to achieve more accurate reconstruction to the original full precision convolutional layer. Note that when  $K = 1$ , it corresponds to directly binarize the floating-point convolutional layer (Fig. 1 (b)). However, with more branches (a larger  $K$ ), we are expected to achieve more accurate approximation with more complex transformations.

Different from [37], we remove the floating-point scalars for two reasons. First, the scalar can be absorbed into batch normalization layers. Second, we empirically observe that

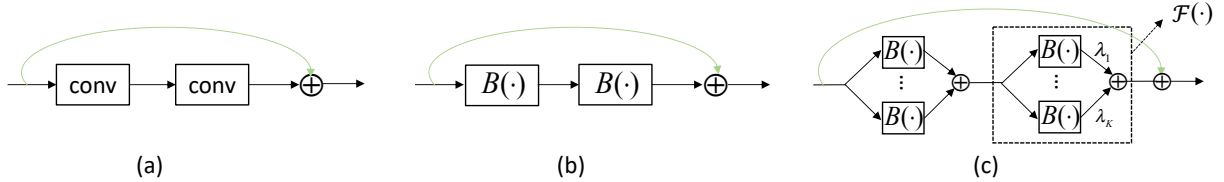


**Fig. 1:** Overview of the baseline binarization method and the proposed layer-wise binary decomposition. We take one residual block with two convolutional layers for illustration. For convenience, we omit batch normalization and nonlinearities. (a): The floating-point residual block. (b): Direct binarization of a full-precision block. (c): Layer-wise binary decomposition in Eq. (3), where we use a set of binary convolutional layers  $B(\cdot)$  to approximate a floating-point convolutional layer.

the learnt scales for different branches differ a little and removing them does not influence the performance.

During the inference, the homogeneous  $K$  bases can be parallelizable and thus the structure is hardware friendly. This will bring significant gain in speed-up of the inference. Specifically, the bitwise XNOR operation and bit-counting can be performed in a parallel of 64 by the current generation of CPUs [17], [73]. We just need to calculate  $K$  binary convolutions and  $K$  full-precision additions. As a result, the speed-up ratio  $\sigma$  for a convolutional layer can be calculated as:

$$\begin{aligned} \sigma &= \frac{c_{in} \cdot c_{out} \cdot w \cdot h \cdot w_{in} \cdot h_{in}}{\frac{1}{64}(Kc_{in} \cdot c_{out} \cdot w \cdot h \cdot w_{in} \cdot h_{in}) + Kc_{out} \cdot w_{out} \cdot h_{out}}, \\ &= \frac{64}{K} \cdot \frac{c_{in} \cdot w \cdot h \cdot w_{in} \cdot h_{in}}{c_{in} \cdot w \cdot h \cdot w_{in} \cdot h_{in} + 64w_{out} \cdot h_{out}}. \end{aligned} \quad (4)$$

We take one layer in ResNet for example. If we set  $c_{in} = 256$ ,  $w \times h = 3 \times 3$ ,  $w_{in} = h_{in} = w_{out} = h_{out} = 28$ ,  $K = 5$ , then it can reach  $12.45 \times$  speedup. But in practice, each branch can be implemented in parallel. And the actual speedup ratio is also influenced by the process of memory read and thread communication.

### 3.2.2 Group-wise binary decomposition

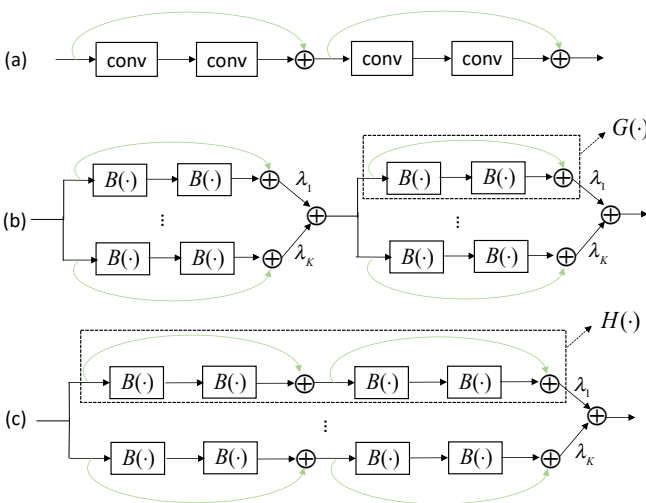


**Fig. 2:** Illustration of the proposed group-wise binary decomposition strategy. We take two residual blocks for description. (a): The floating-point residual blocks. (b): Basic group-wise binary decomposition in Eq. (5), where we approximate a whole block with a linear combination of binary blocks  $G(\cdot)$ . (c): We approximate a whole group with homogeneous binary bases  $H(\cdot)$ , where each group consists of several blocks. This corresponds to Eq. (6).

In the layer-wise approach, we approximate each layer with multiple branches of binary layers. Note each branch will introduce a certain amount of error and the error may accumulate due to the aggregation of multi-branches. As a result, this strategy may incur severe quantization errors and bring large deviation for gradients during back-propagation. To alleviate the above issue, we further propose a more flexible decomposition strategy called group-wise binary decomposition, to preserve more structural information during approximation.

To explore the group-structure decomposition, we first consider a simple case where each group consists of only one block. Then, the layer-wise approximation strategy can be easily extended to the group-wise case. As shown in Fig. 2 (b), similar to the layer-wise case, each floating-point group is decomposed into multiple binary groups. However, each group  $G_i(\cdot)$  is a binary block which consists of several binary convolutions and fixed-point operations (i.e., AddTensor). For example, we can set  $G_i(\cdot)$  as the basic residual block [2] which is shown in Fig. 2 (a). Considering the residual architecture, we can decompose  $\mathcal{F}(\mathbf{x})$  by extending Eq. (3) as:

$$\mathcal{F}(\mathbf{x}) = \frac{1}{K} \sum_{i=1}^K G_i(\mathbf{x}), \quad (5)$$

where  $\lambda_i$  is the combination coefficient to be learned. In Eq. (5), we use a linear combination of homogeneous binary bases to approximate one group, where each base  $G_i$  is a binarized block. Thus, we effectively keep the original residual structure in each base to preserve the network capacity. As shown in Sec. 5.2.1, the group-wise decomposition strategy performs much better than the simple layer-wise approximation.

Furthermore, the group-wise approximation is flexible. We now analyze the case where each group may contain different number of blocks. Suppose we partition the network into  $P$  groups and it follows a simple rule that each group must include one or multiple complete residual building blocks. For the  $p$ -th group, we consider the blocks set  $T \in \{T_{p-1} + 1, \dots, T_p\}$ , where the index  $T_{p-1} = 0$  if  $p = 1$ . We can extend Eq. (5) into multiple blocks format:

$$\begin{aligned} \mathcal{F}(\mathbf{x}_{T_{p-1}+1}) &= \frac{1}{K} \sum_{i=1}^K H_i(\mathbf{x}), \\ &= \sum_{i=1}^K G_i^{T_p} (G_i^{T_p-1} (\dots (G_i^{T_{p-1}+1} (\mathbf{x}_{T_{p-1}+1}) \dots))), \end{aligned} \quad (6)$$

where  $H(\cdot)$  is a cascade of consequent blocks which is shown in Fig. 2 (c). Based on  $\mathcal{F}(\cdot)$ , we can efficiently construct a network by stacking these groups and each group

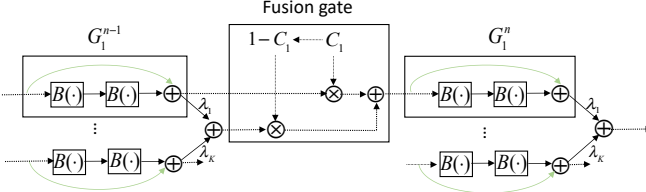


Fig. 3: Illustration of the soft connection between two neighbouring blocks. For convenience, we only illustrate the fusion strategy for one branch.

may consist of one or multiple blocks. Different from Eq. (5), we further expose a new dimension on each base, which is the number of blocks. This greatly increases the structure space and the flexibility of decomposition. We illustrate several possible connections in Fig. 7 and further describe how to learn the decomposition in Sec. 3.2.3.

### 3.2.3 Learning for decomposition

There is a significant challenge involved in Eq. (6). Note that the network has  $N$  blocks and the possible number of connections is  $2^N$ . Clearly, it is not practical to enumerate all possible structures during the training. Here, we propose to solve this problem by learning the structures for decomposition dynamically. We introduce in a fusion gate as the soft connection between blocks  $G(\cdot)$ . To this end, we first define the input of the  $i$ -th branch for the  $n$ -th block as:

$$\begin{aligned} C_i^n &= \text{sigmoid}(\theta_i^n), \\ x_i^n &= C_i^n \odot G_i^{n-1}(x_i^{n-1}) \\ &\quad + (1 - C_i^n) \odot \sum_{j=1}^K G_j^{n-1}(x_j^{n-1}), \end{aligned} \quad (7)$$

where  $\theta \in \mathbb{R}^K$  is a learnable parameter vector,  $C_i^n$  is a gate scalar and  $\odot$  is the Hadamard product. And we empirically observe that using a scalar  $\theta$  that shares among branches does not influence the performance.

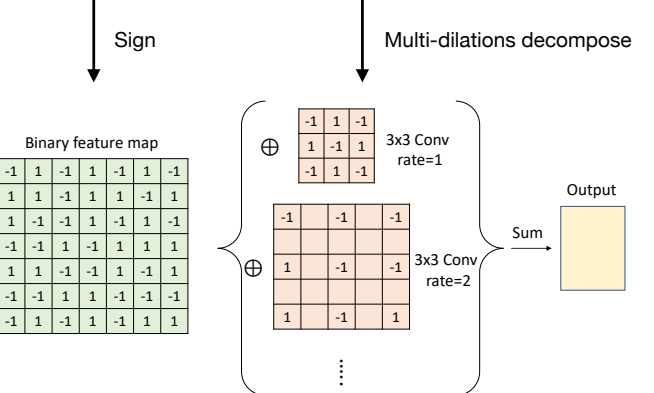
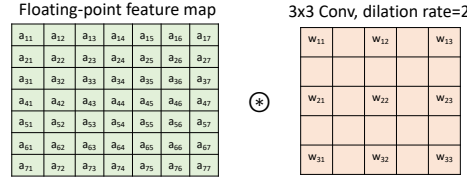
Here, the branch input  $x_i^n$  is a weighted combination of two paths. The first path is the output of the corresponding  $i$ -th branch in the  $(n-1)$ -th block, which is a direct connection. The second path is the aggregation output of the  $(n-1)$ -th block. The detailed structure is shown in Fig. 3. In this way, we make more information flow into the branch and increase the gradient paths for improving the convergence of BNNs.

**Remarks:** For the extreme case when  $\sum_{i=1}^K C_i^n = 0$ , Eq. (7) will be reduced to Eq. (5) which means we approximate the  $(n-1)$ -th and the  $n$ -th block independently. When  $\sum_{i=1}^K C_i^n = K$ , Eq. (7) is equivalent to Eq. (6) and we set  $H(\cdot)$  to be two consequent blocks and approximate the group as a whole. Interestingly, when  $\sum_{n=1}^N \sum_{i=1}^K C_i^n = NK$ , it corresponds to set  $H(\cdot)$  in Eq. (6) to be a whole network and directly ensemble  $K$  binary models.

### 3.3 Extension to semantic segmentation

The key message conveyed in the proposed method is that, although each binary branch has a limited modeling capability, aggregating them together leads to a powerful model. In this section, we show that this principle can be

(a): The conventional floating-point dilated convolution.



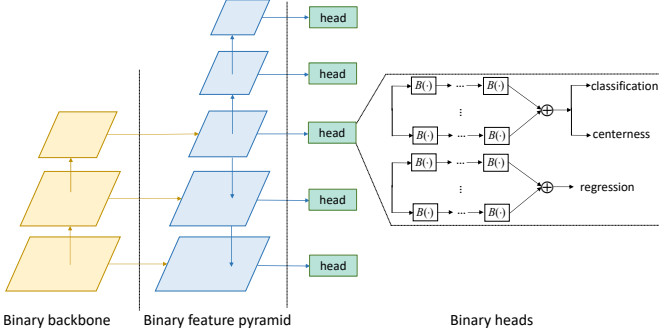
(b): The proposed Binary Parallel Atrous Convolution (BPAC).

Fig. 4: The comparison between conventional dilated convolution and BPAC. For expression convenience, the group only has one convolutional layer.  $\otimes$  is the convolution operation and  $\oplus$  indicates the XNOR-popcount operations. (a): The original floating-point dilated convolution. (b): We decompose the floating-point atrous convolution into a combination of binary bases, where each base uses a different dilated rate. We sum the output features of each binary branch as the final representation.

applied to tasks other than image classification. In particular, we consider semantic segmentation which can be deemed as a dense pixel-wise classification problem. In the state-of-the-art semantic segmentation network, the atrous convolutional layer [26] is an important building block, which performs convolution with a certain dilation rate. To directly apply the proposed method to such a layer, one can construct multiple binary atrous convolutional branches with the same structure and aggregate results from them. However, we choose not to do this but propose an alternative strategy: we use different dilation rates for each branch. In this way, the model can leverage multiscale information as a *by-product of the network branch decomposition*. It should be noted that this scheme does not incur any additional model parameters and computational complexity compared with the naive binary branch decomposition. The idea is illustrated in Fig. 4 and we call this strategy Binary Parallel Atrous Convolution (**BPAC**).

In this work, we use the same ResNet backbone in [4], [26] with  $\text{output\_stride}=8$ , where the last two stages employ atrous convolution. In BPAC, we keep  $\text{rates} = \{2, \dots, K+1\}$  and  $\text{rates} = \{6, \dots, K+5\}$  for  $K$  bases in the last two blocks, respectively. Intriguingly, as will be shown in Sec. 5.3, our strategy brings so much benefit that using five binary bases with BPAC achieves similar performance as the original full precision network despite the fact that it saves considerable computational cost.

### 3.4 Extension to object detection



**Fig. 5:** Illustration of the proposed binary detection framework. We partition the whole framework into three parts, including binary backbone, binary feature pyramid and binary heads.

We further generalize Group-Net to the object detection task. We work on the latest one-stage anchor-free detector FCOS [70] as shown in Figure 5. FCOS is built on the multi-level prediction framework FPN [74]. Its main difference between anchor-based detectors is that it directly views locations as training samples which is the same as in FCNs for semantic segmentation instead of using anchor boxes in anchor-based detectors. More details can be referred to the original paper [70].

The overall detection framework consists of backbone, feature pyramid and heads. We directly use the backbone network pretrained on the ImageNet classification task to initialize the detection backbone. For feature pyramid structure, it attaches a  $1 \times 1$  and  $3 \times 3$  convolutional layer at each resolution to adapt the feature maps. Since it lacks of structural information like the backbone network, we therefore apply the layer-wise binary decomposition in Sec. 3.2.1. Furthermore, the FPN heads occupy a large portion of complexity in the whole detection framework. And each head is comprised of several consequent layers which is similar to a basic residual block. To preserve the structural information, following the spirit of group-wise binary decomposition strategy in Sec. 3.2.2, we propose to approximate the head as a whole. The structure is illustrated in Figure 5.

We note that except the last layers for classification, center-ness and regression, other parameters of the heads are not shared across all feature pyramid levels which is the opposite of the full-precision counterpart. The reason can be attributed to the fact that the multi-level semantic information is represented by activation magnitude at different pyramid levels. In the full-precision setting, the shared heads are enough to adapt the different magnitude for classification and regression. However, in the binary setting, the feature magnitude is at the same scale across the pyramid levels since the activations are constrained to  $\{-1, 1\}$ . With the same input magnitude, the heads should learn independent parameters to capture multi-level information. More optimization details are explained in Sec. 5.4.

## 4 DISCUSSIONS

**Complexity analysis:** A comprehensive comparison of various quantization approaches over complexity and storage

is shown in Table 1. For example, in the previous state-of-the-art binary model ABC-Net [29], each convolutional layer is approximated using  $K$  weight bases and  $K$  activation bases, which needs to calculate  $K^2$  times binary convolution. In contrast, we just need to approximate several groups with  $K$  structural bases. As reported in Sec. 5.1, we save approximate  $K$  times computational complexity while still achieving comparable Top-1 accuracy. Since we use  $K$  structural bases, the number of parameters increases by  $K$  times in comparison to the full-precision counterpart. But we still save memory bandwidth by  $32/K$  times since all the weights are binary in our paper. For our approach, there exists element-wise operations between each group, so the computational complexity saving is slightly less than  $\frac{64}{K} \times$ .

**Differences of Group-net from fixed-point methods:** The proposed Group-net with  $K$  bases is different from the  $K$ -bit fixed-point approaches [10], [19], [22], [24].

We first show how the inner product between fixed-point weights and activations can be computed by bitwise operations. Let a weight vector  $\mathbf{w} \in \mathbb{R}^M$  be encoded by a vector  $\mathbf{b}_i^w \in \{-1, 1\}^M$ ,  $i = 1, \dots, K$ . Assume we also quantize activations to  $K$ -bit. Similarly, the activations  $\mathbf{x}$  can be encoded by  $\mathbf{b}_j^a \in \{-1, 1\}^M$ ,  $j = 1, \dots, K$ . Then, the convolution can be written as

$$Q_K(\mathbf{w}^T)Q_K(\mathbf{x}) = \sum_{i=0}^{K-1} \sum_{j=0}^{K-1} 2^{i+j} (\mathbf{b}_i^w \oplus \mathbf{b}_j^a), \quad (8)$$

where  $Q_K(\cdot)$  is any quantization function<sup>1</sup>.

During the inference, it needs to first get the encoding  $\mathbf{b}_j^a$  for each bit by looking up the quantization intervals. Then, it calculates and sums over  $K^2$  times  $\text{xnor}(\cdot)$  and  $\text{popcount}(\cdot)$ . The complexity is about  $O(K^2)$ . Note that the output range for a single output shall be  $[-(2^K - 1)^2 M, (2^K - 1)^2 M]$ .

In contrast, we directly obtain  $\mathbf{b}_j^a$  via  $\text{sign}(\mathbf{x})$ . Moreover, since we just need to calculate  $K$  times  $\text{xnor}(\cdot)$  and  $\text{popcount}(\cdot)$  (see Eq. (3)), and then sum over the outputs, the computational complexity is  $O(K)$ . For binary convolution, its output range is  $\{-1, 1\}$ . So the value range for each element after summation is  $[-KM, KM]$ , in which the number of distinct values is much less than that in fixed-point methods.

In summary, compared with  $K$ -bit fixed-point methods, Group-Net with  $K$  bases just needs  $\sqrt{K}$  computational complexity and saves  $(2^K - 1)^2 / K$  accumulator bandwidth. Even  $\sqrt{K}$ -bit fixed-point quantization requires more memory bandwidth to feed signal in SRAM or in registers.

**Differences of Group-net from multiple binarizations methods:** In ABC-Net [29], a linear combination of binary weight/activations bases are obtained from the full-precision weights/activations without being directly learned. In contrast, we directly design the binary network structure, where binary weights are end-to-end optimized. [27], [28], [30], [31] propose to recursively approximate the residual error and obtain a series of binary maps corresponding to different quantization scales. However, it is a sequential process which cannot be paralleled. And all multiple binarizations methods belong to local

1. For simplicity, we only consider uniform quantization in this paper.

**TABLE 1:** Computational complexity and storage comparison of different quantization approaches.  $F$ : full-precision,  $B$ : binary,  $Q_K$ :  $K$ -bit quantization.

| Model                        | Weights           | Activations  | Operations                     | Memory saving              | Computation Saving        |
|------------------------------|-------------------|--------------|--------------------------------|----------------------------|---------------------------|
| Full-precision DNN           | $F$               | $F$          | $+, -, \times$                 | 1                          | 1                         |
| [16], [17]                   | $B$               | $B$          | XNOR-popcount                  | $\sim 32 \times$           | $\sim 64 \times$          |
| [21], [75]                   | $B$               | $F$          | $+, -$                         | $\sim 32 \times$           | $\sim 2 \times$           |
| [39], [76]                   | $Q_K$             | $F$          | $+, -, \times$                 | $\sim \frac{32}{K} \times$ | $< 2 \times$              |
| [10], [19], [22], [24]       | $Q_K$             | $Q_K$        | $+, -, \times$                 | $\sim \frac{32}{K} \times$ | $< \frac{64}{K^2} \times$ |
| [27], [28], [29], [30], [31] | $K \times B$      | $K \times B$ | $+, -, \times$ , XNOR-popcount | $\sim \frac{32}{K} \times$ | $< \frac{64}{K^2} \times$ |
| Group-Net                    | $K \times (B, B)$ |              | $+, -, \times$ , XNOR-popcount | $\sim \frac{32}{K} \times$ | $< \frac{64}{K} \times$   |

tensor approximation. In contrast to value approximation, we propose a structure approximation approach to mimic the full-precision network. Moreover, tensor-based methods are tightly designed to local value approximation and are hardly generalized to other tasks accordingly. In addition, our structure decomposition strategy achieves much better performance than tensor-level approximation as shown in Sec. 5.2.1. More discussions are provided in Sec. S2 in the supplementary file.

**Relation to ResNeXt [77]:** The homogeneous multi-branch architecture design shares the spirit of ResNeXt and enjoys the advantage of introducing a “cardinality” dimension. However, our objectives are totally different. ResNeXt aims to increase the capacity while maintaining the complexity. To achieve this, it first divides the input channels into groups and perform efficient group convolutions implementation. Then all the group outputs are aggregated to approximate the original feature map. In contrast, we first divide the network into groups and directly replicate the floating-point structure for each branch while both weights and activations are binarized. In this way, we can reconstruct the full-precision structure via aggregating a set of low-precision transformations for complexity reduction in the energy-efficient hardware. Furthermore, our structured transformations are not restricted to a single residual block as in ResNeXt.

**Group-Net has strong flexibility:** The group-wise approximation approach can be efficiently integrated with Neural Architecture Search (NAS) frameworks [34], [35], [36], [50], [78] to explore the optimal architecture. For instance, based on Group-Net, we can further add the number of bases, depth as well as the resolution into the search space following [79]. The proposed approach can also be combined with knowledge distillation strategy as in [10], [19]. In this way, we expect to further decrease the number of bases while maintaining the performance.

## 5 EXPERIMENT

We define several methods for comparison as follows: **LBD**: It implements the layer-wise binary decomposition strategy described in Sec. 3.2.1. **Group-Net**: It implements the full model with learnt soft connections described in Sec. 3.2.3. Following Bi-Real Net [73], [80], we apply shortcut bypassing every binary convolution to improve the convergence. Note that due to the binary convolution, skip connections are high-precision which can be efficiently implemented using fixed-point addition. **Group-Net\*\***: Based on Group-Net, we keep the  $1 \times 1$  downsampling convolution to high-precision (i.e., 8-bit) similar to [73], [81].

### 5.1 Evaluation on ImageNet

The proposed method is first evaluated on ImageNet (ILSVRC2012) [82] dataset. ImageNet is a large-scale dataset which has  $\sim 1.2M$  training images from 1K categories and 50K validation images. Several representative networks are tested: ResNet-18 [2], ResNet-34 and ResNet-50. As discussed in Sec. 4, binary approaches and fixed-point approaches differ a lot in computational complexity as well as storage consumption. So we compare the proposed approach with binary neural networks in Table 2 and fixed-point approaches in Table 3, respectively.

#### 5.1.1 Implementation details

As in [10], [17], [22], [23], we quantize the weights and activations of all convolutional layers except that the first and the last layer are quantized to 8-bit. In all ImageNet experiments, training images are resized to  $256 \times 256$ , and a  $224 \times 224$  crop is randomly sampled from an image or its horizontal flip, with the per-pixel mean subtracted. We do not use any further data augmentation in our implementation. We use a simple single-crop testing for standard evaluation. No bias term is utilized. Training is divided into two steps. We first pretrain the full-precision model as initialization and fine-tune the binary counterpart. For pretraining, we use SGD with a initial learning rate of 0.05, a momentum of 0.9 and a weight decay of 1e-4. We use  $\text{Tanh}(\cdot)$  as nonlinearity instead of  $\text{ReLU}(\cdot)$ . For fine-tuning, we use Adam [83] for optimization. For training all binary networks, the mini-batch size and weight decay are set to 256 and 0, respectively. The learning rate starts at 5e-4. For both steps, the learning rate is decayed twice by multiplying 0.1 at the 25th and 35th epoch, and we train a maximum 40 epochs in each step. Following [10], [23], no dropout is used due to binarization itself can be treated as a regularization. We apply layer-reordering to the networks as: Sign  $\rightarrow$  Conv  $\rightarrow$  ReLU  $\rightarrow$  BN. Inserting  $\text{ReLU}(\cdot)$  after convolution is important for convergence. Our simulation implementation is based on Pytorch [84].

#### 5.1.2 Comparison with binary neural networks

Since we employ binary weights and binary activations, we directly compare to the previous state-of-the-art binary approaches, including BNN [16], XNOR-Net [17], Bi-Real Net [73] and ABC-Net [29]. We report the results in Table 2 and summarize the following points. 1): The most comparable baseline for Group-Net is ABC-Net. As discussed in Sec. 4, we save considerable computational complexity while still achieving better performance compared to ABC-Net. In comparison to directly binarizing networks, Group-Net achieves much better performance but needs  $K$  times

**TABLE 2:** Comparison with the state-of-the-art binary models using ResNet-18, ResNet-34 and ResNet-50 on ImageNet. All the comparing results are directly cited from the original papers. The metrics are Top-1 and Top-5 accuracy.

| Model     | Full    | BNN  | XNOR | Bi-Real Net | ABC-Net (25 bases) | Group-Net (5 bases) | Group-Net** (5 bases) | Group-Net (8 bases) |
|-----------|---------|------|------|-------------|--------------------|---------------------|-----------------------|---------------------|
| ResNet-18 | Top-1 % | 69.7 | 42.2 | 51.2        | 56.4               | 65.0                | 64.8                  | 67.0                |
|           | Top-5 % | 89.4 | 67.1 | 73.2        | 79.5               | 85.9                | 85.7                  | 88.0                |
| ResNet-34 | Top-1 % | 73.2 | -    | -           | 62.2               | 68.4                | 68.5                  | 70.5                |
|           | Top-5 % | 91.4 | -    | -           | 83.9               | 88.2                | 88.0                  | 89.3                |
| ResNet-50 | Top-1 % | 76.0 | -    | -           | -                  | 70.1                | 69.5                  | 71.2                |
|           | Top-5 % | 92.9 | -    | -           | -                  | 89.7                | 88.2                  | 90.0                |

**TABLE 3:** Comparison with the state-of-the-art fixed-point models with ResNet-18 on ImageNet. The metrics are Top-1 and Top-5 accuracy.

| Model                 | W  | A  | Top-1 (%)   | Top-5 (%)   |
|-----------------------|----|----|-------------|-------------|
| Full-precision        | 32 | 32 | 69.7        | 89.4        |
| Group-Net** (4 bases) | 1  | 1  | <b>66.3</b> | <b>86.6</b> |
| Group-Net (4 bases)   | 1  | 1  | 64.2        | 85.6        |
| LQ-Net [24]           | 2  | 2  | 64.9        | 85.9        |
| DoReFa-Net [22]       | 2  | 2  | 62.6        | 84.4        |
| SYQ [86]              | 1  | 8  | 62.9        | 84.6        |

more storage and complexity. However, the  $K$  homogeneous bases can be easily parallelized on the real chip. In summary, our approach achieves the best trade-off between computational complexity and prediction accuracy. 2): By comparing Group-Net\*\* (5 bases) and Group-Net (8 bases), we can observe comparable performance. *It justifies keeping  $1 \times 1$  downsampling layers to high-precision is crucial for preserving the performance.* 3): For Bottleneck structure in ResNet-50, we find larger quantization error than the counterparts using basic blocks with  $3 \times 3$  convolutions in ResNet-18 and ResNet-34. The similar observation is also claimed by [85]. We assume that this is mainly attributable to the  $1 \times 1$  convolutions in Bottleneck. The reason is  $1 \times 1$  filters are limited to two states only (either 1 or  $-1$ ) and they have very limited learning power. Moreover, the bottleneck structure reduces the number of filters significantly, which means the gradient paths are greatly reduced. In other words, it blocks the gradient flow through BNNs. *Even though the bottleneck structure can benefit full-precision training, it is really needed to be redesigned in BNNs. To increase gradient paths, the  $1 \times 1$  convolutions should be removed.*

### 5.1.3 Comparison with fix-point approaches

Since we use  $K$  binary group bases, we compare our approach with at least  $\sqrt{K}$ -bit fix-point approaches. In Table 3, we compare our approach with the state-of-the-art fixed-point approaches DoReFa-Net [22], SYQ [86] and LQ-Nets [24]. As described in Sec. 4,  $K$  binarizations are more superior than the  $\sqrt{K}$ -bit width quantization with respect to the resource consumption. Here, we set  $K=4$ . DoReFa-Net and LQ-Nets use 2-bit weights and 2-bit activations. SYQ employs binary weights and 8-bit activations. All the comparison results are directly cited from the corresponding papers. LQ-Nets is the current best-performing fixed-point approach and its activations have a long-tail distribution. We can observe that Group-Net requires less memory bandwidth while still achieving comparable accuracy with LQ-Nets.

**TABLE 4:** Comparison with Group-Net and LBD using ResNet-18 on ImageNet. The metrics are Top-1 and Top-5 accuracy.

| Model          | Bases | Top-1 %     | Top-5 %     |
|----------------|-------|-------------|-------------|
| Full-precision | 1     | 69.7        | 89.4        |
| Group-Net      | 5     | <b>64.8</b> | <b>85.7</b> |
| LBD            | 5     | 57.6        | 79.7        |

## 5.2 Ablation study on ImageNet classification

### 5.2.1 Layer-wise vs. group-wise binary decomposition

We explore the difference between layer-wise and group-wise design strategies in Table 4. By comparing the results, we find Group-Net outperforms LBD by 7.2% on the Top-1 accuracy. Note that LBD approach can be treated as a kind of *tensor approximation* which has similarities with multiple binarizations methods in [27], [28], [29], [30], [31] and the differences are described in Sec. 4. It strongly shows the necessity for employing the group-wise decomposition strategy to get promising results. We speculate that this significant gain is partly due to the preserved block structure in binary bases. It also proves that apart from designing accurate binarization function, it is also essential to design appropriate structure for BNNs.

### 5.2.2 Effect of the soft gate

In this section, we further analysis the effect of soft gate described in Sec. 3.2. We show the convergence curves in Figure 6 and quantitative results in Table 5. From the results, we can observe consistent accuracy improvement for various architectures. This shows that increasing the gradient paths and learning the information flow within BNNs is important for maintaining the performance. For instance, on ResNet-34, learning the soft gates can improve the Top-1 accuracy by 2.2%.

**TABLE 5:** The effect of soft gates on ImageNet.

| Model     | Full    | Group-Net (w/o softgates) | Group-Net |
|-----------|---------|---------------------------|-----------|
| ResNet-18 | Top-1 % | 69.7                      | 64.2      |
|           | Top-5 % | 89.4                      | 85.0      |
| ResNet-34 | Top-1 % | 73.2                      | 66.3      |
|           | Top-5 % | 91.4                      | 86.2      |
| ResNet-50 | Top-1 % | 76.0                      | 67.5      |
|           | Top-5 % | 92.9                      | 86.7      |

### 5.2.3 Effect of the number of bases

We further explore the influence of number of bases  $K$  to the final performance in Table 6. When the number is set to 1, it corresponds to directly binarize the original full-precision network and we observe apparent accuracy drop compared to its full-precision counterpart. With more bases employed, we can find the performance steadily increases. The reason can be attributed to the better fitting of the

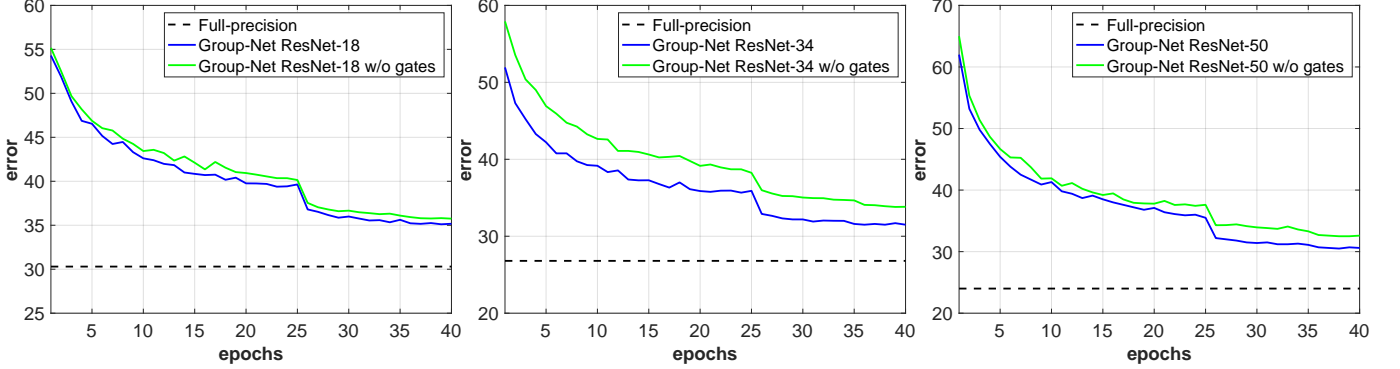


Fig. 6: Validation curves for ImageNet classification.

TABLE 6: Validation accuracy of Group-Net on ImageNet with different number of bases. All cases are based on the ResNet-18 network with binary weights and activations.

| Model          | Bases | Top-1 % | Top-5 % | Top-1 gap % | Top-5 gap % |
|----------------|-------|---------|---------|-------------|-------------|
| Full-precision | 1     | 69.7    | 89.4    | -           | -           |
| Group-Net      | 1     | 56.4    | 79.5    | 13.3        | 9.9         |
| Group-Net      | 3     | 62.5    | 84.2    | 7.2         | 5.2         |
| Group-Net      | 5     | 64.8    | 85.7    | 4.9         | 3.7         |

floating-point structure, which is a trade-off between accuracy and complexity. It can be expected that with enough bases, the network should have the capacity to approximate the full-precision network precisely. With the multi-branch group-wise design, we can achieve high accuracy while still significantly reducing the inference time and power consumption. Interestingly, each base can be implemented using small resource and the parallel structure is quite friendly to FPGA/ASIC.

#### 5.2.4 Effect of the group space

To show the importance of the structure design, we define more methods for comparison as follows: **GBD v1**: We implement with the group-wise binary decomposition strategy, where each base consists of one block. It corresponds to the approach described in Eq. (5) and is illustrated in Fig. 7 (a). **GBD v2**: Similar to GBD v1, the only difference is that each group base has two blocks. It is illustrated in Fig. 7 (b) and is explained in Eq. (6). **GBD v3**: It is an extreme case where each base is a whole network, which can be treated as an ensemble of a set of binary networks. This case is shown in Fig. 7 (d).

We present the results in Table 7. We observe that learning the soft connections between each group results in the best performance on ResNet-18. And methods based on hard connections perform relatively worse. Moreover, different architectures can have a great impact on the performance. For example, the Top-1 gap between “GBD v2” and “GBD v3” is 3% even though their complexity is nearly the same. From the results, we can conclude that designing compact binary structure is essential for highly accurate classification.

### 5.3 Evaluation on semantic segmentation

In this section, we further evaluate Group-Net on the PASCAL VOC 2012 semantic segmentation benchmark [87]

TABLE 7: Comparisons between several group-wise decomposition strategies. Top-1 and Top-5 accuracy gaps to the corresponding full-precision ResNet-18 network are also reported.

| Model          | Bases | Top-1 % | Top-5 % | Top-1 gap % | Top-5 gap % |
|----------------|-------|---------|---------|-------------|-------------|
| Full-precision | 1     | 69.7    | 89.4    | -           | -           |
| Group-Net      | 5     | 64.8    | 85.7    | 4.9         | 3.7         |
| GBD v1         | 5     | 63.0    | 84.8    | 6.7         | 4.6         |
| GBD v2         | 5     | 62.2    | 84.1    | 7.5         | 5.3         |
| GBD v3         | 5     | 59.2    | 82.3    | 10.5        | 7.1         |

which contains 20 foreground object classes and one background class. The original dataset contains 1,464 (*train*), 1,449 (*val*) and 1,456 (*test*) images. The dataset is augmented by the extra annotations from [88], resulting in 10,582 training images. The performance is measured in terms of averaged pixel intersection-over-union (mIOU) over 21 classes.

**Implementation details.** Our experiments are based on FCN [3]. For both FCN-32s and FCN-16s, we adjust the dilation rates of the last two stages in ResNet with atrous convolution to make the output stride equal to 8. We first pretrain the binary backbone network on ImageNet dataset and fine-tune it on PASCAL VOC. During fine-tuning, we use Adam with initial learning rate=1e-4, weight decay=0 and batch size=16. We set the number of bases  $K = 5$  in experiments. We train 40 epochs in total and decay the learning rate by a factor of 10 at 20 and 30 epochs. We do not add any auxiliary loss and ASPP. We empirically observe full-precision FCN under dilation rates (4, 8) in last two stages achieves the best performance.

#### 5.3.1 Experiments on FCN

TABLE 8: Performance of Group-Net on PASCAL VOC 2012 validation set with FCN.

| Model              | Full-precision | mIOU | $\Delta$ |
|--------------------|----------------|------|----------|
| ResNet-18, FCN-32s | Full-precision | 64.9 | -        |
|                    | LQ-Net (3-bit) | 62.5 | 2.4      |
|                    | Group-Net      | 60.5 | 4.4      |
| ResNet-18, FCN-16s | Full-precision | 67.3 | -        |
|                    | LQ-Net (3-bit) | 65.1 | 2.2      |
|                    | Group-Net      | 62.7 | 4.6      |
| ResNet-34, FCN-32s | Full-precision | 72.7 | -        |
|                    | LQ-Net (3-bit) | 70.4 | 2.3      |
|                    | Group-Net      | 68.2 | 4.5      |
| ResNet-50, FCN-32s | Full-precision | 73.1 | -        |
|                    | LQ-Net (3-bit) | 70.7 | 2.4      |
|                    | Group-Net      | 68.3 | 4.8      |

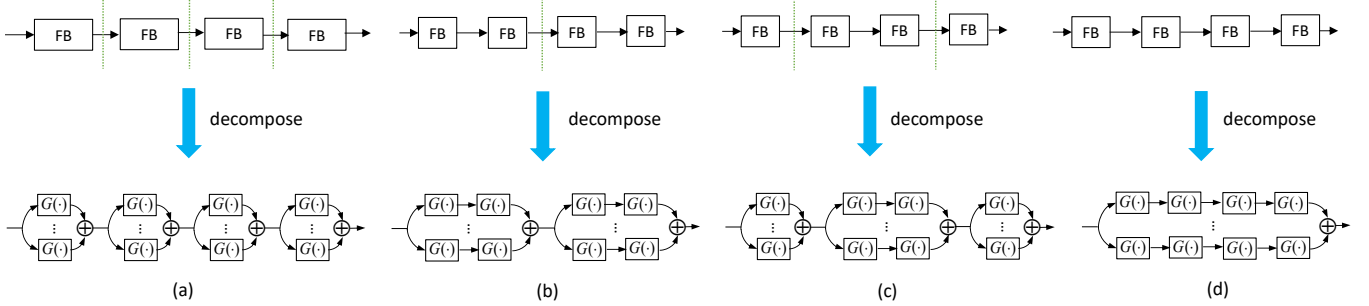


**Fig. 7:** Illustration of several possible group-wise architectures. We assume the original full-precision network comprises four blocks. “FB” represents the floating-point block.  $G(\cdot)$  is defined in Sec. 3.2.2, which represents a binary block. We omit the skip connections for convenience. (a): Each group comprises one block and we approximate each floating-point block with a set of binarized blocks. (b): Decompose the network into groups, where each group contains two blocks. Then we approximate each floating-point group using a set of binarized groups. (c): Each group contains different number of blocks. (d): An extreme case. We directly decompose the whole floating-point network into an ensemble of several binary networks.

**TABLE 9:** Performance of Group-Net with BPAC on PASCAL VOC 2012 validation set with FCN.

| Model              | mIOU                                  |
|--------------------|---------------------------------------|
| ResNet-18, FCN-32s | Full-precision (multi-dilations) 67.6 |
|                    | Group-Net + BPAC 63.8                 |
|                    | Group-Net** + BPAC <b>65.1</b>        |
| ResNet-18, FCN-16s | Full-precision (multi-dilations) 70.1 |
|                    | Group-Net + BPAC 66.3                 |
|                    | Group-Net** + BPAC <b>67.7</b>        |
| ResNet-34, FCN-32s | Full-precision (multi-dilations) 75.0 |
|                    | Group-Net + BPAC 71.2                 |
|                    | Group-Net** + BPAC <b>72.8</b>        |
| ResNet-50, FCN-32s | Full-precision (multi-dilations) 75.5 |
|                    | Group-Net + BPAC 71.8                 |
|                    | Group-Net** + BPAC <b>72.8</b>        |

The main results are reported in Table 8 and Table 9. From the results in Table 8, we can observe that when all bases using the same dilation rates, there is an obvious performance gap with the full-precision counterpart. This performance drop is consistent with the classification results on ImageNet dataset in Table 2. It proves that the quality of extracted features have a great impact on the segmentation performance. Moreover, we also quantize the backbone network using fixed-point LQ-Nets with 3-bit weights and 3-bit activations. Compared with LQ-Nets, we can achieve comparable performance while saving considerable complexity.

To reduce performance loss, we further employ diverse dilated rates on parallel binary bases to capture the multi-scale information without increasing any computational complexity. This formulates our final approach Group-Net + BPAC in Table 9, which shows significant improvement over the Group-Net counterpart. Moreover, the performance of Group-Net + BPAC is comparable with the full-precision baseline in Table 8, which strongly justifies the flexibility of Group-Net.

In addition, we can observe that Group-Net based on ResNet-50 backbone has the largest relative performance drop. It further shows the widely used bottleneck structure is not suited to BNNs as explained in Sec. 5.1.2.

### 5.3.2 Experiments on DeepLabv3

For training the DeepLabv3 baseline, we use Adam as the optimizer. The initial learning rate for training backbone

**TABLE 10:** The difference for binarizing ASPP with  $\{-1, 1\}$  and  $\{0, 1\}$ .

| Model     | full-precision | $\{0, 1\}$ | $\{-1, 1\}$ |
|-----------|----------------|------------|-------------|
| ResNet-18 | 72.1%          | 63.4%      | 50.8%       |

network is set to  $1e-4$ , and is multiplied by 10 for ASPP module. Similar to image classification, we keep the first layer and last classification layer to 8-bit. We employ the layer-wise approximation in quantizing the ASPP module. We set  $K = 5$  for both backbone and ASPP. The training details are the same with those in FCN except that we use the polynomial decay of learning rate. The results are provided in Table 11.

Moreover, a problem still exists in training binary DeepLabv3. The ASPP module uses large dilation rates for the three  $3 \times 3$  convolutions with  $rates = \{12, 24, 36\}$  when  $output\_stride=8$ . For training BNNs with Eq. (2), we apply one-paddings to constrain activations to  $\{-1, 1\}$ . However, for atrous convolution with large rates, padding ones can introduce high bias and make the optimization difficult. To solve this problem, we instead binarize the activations to  $\{0, 1\}$  following the quantizer in [22]. Note that the numerical difference is only a scalar whether activations are represented by  $\{-1, 1\}$  or  $\{0, 1\}$  in bitwise operations to accelerate the dot products [22], [24]. The importance for binarizing activations to  $\{0, 1\}$  is shown in Table 10.

It is worth noting that the comparable counterpart of DeepLabv3 is the *Group-Net + BPAC* with FCN-32s in Table 9. The main difference is that in the proposed BPAC module, we directly incorporate the multiple dilation rates in the backbone network to capture multi-scale context. In contrast, DeepLabv3 embeds the ASPP module on top of the backbone network. With the same  $output\_stride$ , the computational complexity of FCN is lower than DeepLabv3 since no additional ASPP is needed. With the simpler quantized FCN framework with BPAC, we can achieve comparable or even better performance than quantized DeepLabv3. For example, with the ResNet-34 backbone, GroupNet + BPAC outperforms DeepLabv3 by 4.4 w.r.t mIOU. It also shows that binarization on ASPP is sensitive to the final performance, since the binarization process constrains the feature magnitude to  $\{-1, 1\}$  which causes the multi-scale information loss.

**TABLE 11:** Performance on PASCAL VOC 2012 validation set with DeepLabv3.

| Model     |                 | mIOU (%) | $\Delta$ |
|-----------|-----------------|----------|----------|
| ResNet-18 | Full-precision  | 72.1     | -        |
|           | Backbone        | 66.9     | 5.2      |
|           | Backbone + ASPP | 63.4     | 8.7      |
| ResNet-34 | Full-precision  | 74.4     | -        |
|           | Backbone        | 70.0     | 4.4      |
|           | Backbone + ASPP | 66.2     | 8.2      |
| ResNet-50 | Full-precision  | 76.9     | -        |
|           | Backbone        | 71.8     | 5.1      |
|           | Backbone + ASPP | 68.1     | 8.8      |

**TABLE 12:** Performance on the COCO validation set.

| Model     | AP             | AP <sub>50</sub> | AP <sub>75</sub> | AP <sub>S</sub> | AP <sub>M</sub> | AP <sub>L</sub> |
|-----------|----------------|------------------|------------------|-----------------|-----------------|-----------------|
| ResNet-18 | Full-precision | 27.9             | 45.1             | 28.8            | 15.2            | 30.0            |
|           | Group-Net      | 21.5             | 36.1             | 22.1            | 10.0            | 22.3            |
| ResNet-34 | Full-precision | 32.5             | 50.5             | 34.1            | 17.5            | 35.6            |
|           | Group-Net      | 25.6             | 40.8             | 26.8            | 12.2            | 27.1            |
| ResNet-50 | Full-precision | 36.5             | 55.8             | 39.0            | 21.0            | 40.6            |
|           | Group-Net      | 29.6             | 46.0             | 31.5            | 15.4            | 32.4            |

**TABLE 13:** Performance on COCO test set.

| Model     | AP             | AP <sub>50</sub> | AP <sub>75</sub> | AP <sub>S</sub> | AP <sub>M</sub> | AP <sub>L</sub> |
|-----------|----------------|------------------|------------------|-----------------|-----------------|-----------------|
| ResNet-18 | Full-precision | 28.2             | 45.7             | 29.4            | 14.4            | 29.4            |
|           | Group-Net      | 21.7             | 36.6             | 22.2            | 10.1            | 22.0            |
| ResNet-34 | Full-precision | 32.6             | 50.7             | 34.5            | 16.9            | 34.5            |
|           | Group-Net      | 25.5             | 41.7             | 26.6            | 12.9            | 26.5            |
| ResNet-50 | Full-precision | 36.9             | 56.5             | 39.3            | 20.6            | 39.6            |
|           | Group-Net      | 29.7             | 46.5             | 31.4            | 15.8            | 32.0            |

## 5.4 Evaluation on object detection

In this section, we evaluate Group-Net on the general object detection task. Our experiments are conducted on the large-scale detection benchmark COCO [89]. Following [66], [74], we use the COCO *trainval35k* split (115K images) for training and *minival* split (5K images) for validation. We also report our results on the *test-dev* split (20K images) by uploading our detection results to the evaluation server. In all settings, we set  $K = 5$  for the backbone and  $K = 4$  for the feature pyramid and heads.

**Implementation details.** In specific, the backbone is initialized by the pretrained weights on ImageNet classification. Group-Net is then fine-tuned with Adam with the initial learning rate of 5e-4 and the batch size of 16 for 90,000 iterations. The learning rate is decayed by 10 at iteration 60,000 and 80,000, respectively. Note that we keep updating the BN layers rather than fix them during training. Other hyper-parameters are kept the same with [66], [70].

### 5.4.1 Performance evaluation

We report the performance on the COCO validation set in Table 12 and test set in Table 13, respectively. We can observe that Group-Net achieves promising results over all ResNet architectures. For instance, with the ResNet-18 backbone, the gap of AP is only 6.4 while we save considerable computational complexity. This strongly shows that the proposed Group-Net is a general approach that can be extended on many fundamental computer vision tasks. Furthermore, we highlight that we are the first to explore binary neural networks on object detection in the literature.

We further analysis the memory and computation saving in Table 14. Since we work on the quantization scheme, the floating-point complexity metric FLOPs is not suitable for quantization. Therefore, we also follow the metric in UniQ [90], where BOPs is used to measure the number of

bit-operations in a neural network. For the 18-layer, 34-layer and 50-layer networks, Group-Net reduces the memory usage by  $7.84\times$ ,  $9.86\times$  and  $9.50\times$ , respectively, and it achieves BOPs reduction of  $12.9\times$ ,  $16.5\times$  and  $17.1\times$  in comparison with the full-precision counterpart. Moreover, we directly count the total number of BOPs in the network. In practice, the binary bases are implemented in parallel and actual speed varies according to different hardware platforms.

### 5.4.2 Detection components analysis

We further analysis the affect of quantizing the backbone, feature pyramid and heads to the final performance, respectively. The results are reported in Table 15. From the results, we can summarize two instructive statements.

- We can observe that binarizing the backbone and the feature pyramid only downgrades the performance by a small margin. However, binarizing heads can cause an obvious AP drop. It can be attributed to that heads are responsible for adapting the extracted multi-level features to the classification and regression objectives. As a result, its representability is crucial for robust detectors. However, the multi-level information is undermined when being constrained to  $\{-1, 1\}$ . *This shows that the detection modules other than the backbone are sensitive for quantization, which can be a promising direction in the future work.*
- By comparing the results with respect to weight sharing, we observe the original sharing heads strategy that widely used in full-precision detection frameworks performs extremely bad in the binary setting. In specific, with ResNet-18 backbone, the AP gap between with and without weight sharing reaches by 8.1. It is worth noting that separating the parameters does not increase any additional computational complexity. Even though the number of parameters are increased (i.e., by  $\sim 4$  times in FPN), the memory consumption is still significantly reduced due to the 1-bit storage.

## 6 CONCLUSION

In this paper, we have explored highly efficient and accurate CNN architectures with binary weights and activations. Specifically, we have proposed to directly decompose the full-precision network into multiple groups and each group is approximated using a set of binary bases which can be optimized in an end-to-end manner. We have also proposed to learn the decomposition automatically.

Experimental results have proved the effectiveness of the proposed approach on the ImageNet classification task. More importantly, we have generalized the proposed Group-Net approach from image classification tasks to more challenging fundamental computer vision tasks, namely dense prediction tasks such as semantic segmentation and object detection. We highlight that we may be among the first few approaches to apply binary neural networks on general semantic segmentation and object detection tasks, and achieve encouraging performance on PASCAL VOC and COCO datasets with binary networks.

TABLE 14: Memory usage, FLOPs and BOPs on object detection.

| Model     |                | Memory usage           | Memory saving | FLOPs                 | FLOPs saving | BOPs                  | BOPs saving |
|-----------|----------------|------------------------|---------------|-----------------------|--------------|-----------------------|-------------|
| ResNet-18 | Full-precision | $8.69 \times 10^8$ bit | 1.0×          | $7.43 \times 10^{10}$ | 1.0×         | $8.36 \times 10^{13}$ | 1.0×        |
|           | Group-Net      | $1.10 \times 10^8$ bit | 7.84×         | $5.98 \times 10^9$    | 12.42×       | $5.04 \times 10^{12}$ | 12.9×       |
| ResNet-34 | Full-precision | $1.19 \times 10^9$ bit | 1.0×          | $9.79 \times 10^{10}$ | 1.0×         | $1.10 \times 10^{14}$ | 1.0×        |
|           | Group-Net      | $1.21 \times 10^8$ bit | 9.86×         | $7.82 \times 10^9$    | 12.52×       | $6.67 \times 10^{12}$ | 16.5×       |
| ResNet-50 | Full-precision | $1.13 \times 10^9$ bit | 1.0×          | $8.35 \times 10^{10}$ | 1.0×         | $1.16 \times 10^{14}$ | 1.0×        |
|           | Group-Net      | $1.19 \times 10^8$ bit | 9.50×         | $6.70 \times 10^9$    | 12.46×       | $6.80 \times 10^{12}$ | 17.1×       |

TABLE 15: Performance on COCO validation set with different binarized components.

| Model     |   | AP   | AP <sub>50</sub> | AP <sub>75</sub> | AP <sub>S</sub> | AP <sub>M</sub> | AP <sub>L</sub> |
|-----------|---|------|------------------|------------------|-----------------|-----------------|-----------------|
| ResNet-18 | Full-precision                                  | 27.9 | 45.1             | 28.8             | 15.2            | 30.0            | 37.5            |
|           | Backbone  | 27.8 | 44.5             | 28.9             | 14.7            | 29.8            | 37.0            |
|           | Backbone + Feature pyramid                      | 26.9 | 43.1             | 28.2             | 14.8            | 28.7            | 35.4            |
|           | Backbone + Feature pyramid + Heads (shared)     | 13.4 | 30.1             | 10.9             | 5.8             | 15.5            | 20.1            |
| ResNet-34 | Backbone + Feature pyramid + Heads (w/o shared) | 21.5 | 36.1             | 22.1             | 10.0            | 22.3            | 29.9            |
|           | Full-precision                                  | 32.5 | 50.5             | 34.1             | 17.5            | 35.6            | 42.2            |
|           | Backbone  | 30.6 | 47.7             | 32.2             | 16.5            | 33.0            | 40.7            |
|           | Backbone + Feature pyramid + Heads (w/o shared) | 25.6 | 40.8             | 26.8             | 12.2            | 27.1            | 34.3            |

## ACKNOWLEDGMENTS

L. Liu was in part supported by ARC DECRA Fellowship DE170101259. M. Tan was partially supported by National Natural Science Foundation of China (NSFC) 61602185, Program for Guangdong Introducing Innovative and Entrepreneurial Teams 2017ZT07X183.

## REFERENCES

- [1] A. Krizhevsky, I. Sutskever, and G. E. Hinton, "Imagenet classification with deep convolutional neural networks," in *Proc. Adv. Neural Inf. Process. Syst.*, 2012, pp. 1097–1105.
- [2] K. He, X. Zhang, S. Ren, and J. Sun, "Deep residual learning for image recognition," in *Proc. IEEE Conf. Comp. Vis. Patt. Recogn.*, 2016, pp. 770–778.
- [3] J. Long, E. Shelhamer, and T. Darrell, "Fully convolutional networks for semantic segmentation," in *Proc. IEEE Conf. Comp. Vis. Patt. Recogn.*, 2015, pp. 3431–3440.
- [4] L.-C. Chen, Y. Zhu, G. Papandreou, F. Schroff, and H. Adam, "Encoder-decoder with atrous separable convolution for semantic image segmentation," in *Proc. Eur. Conf. Comp. Vis.*, 2018, pp. 801–818.
- [5] J. Redmon, S. Divvala, R. Girshick, and A. Farhadi, "You only look once: Unified, real-time object detection," in *Proc. IEEE Conf. Comp. Vis. Patt. Recogn.*, 2016, pp. 779–788.
- [6] S. Ren, K. He, R. Girshick, and J. Sun, "Faster r-cnn: Towards real-time object detection with region proposal networks," in *Proc. Adv. Neural Inf. Process. Syst.*, 2015, pp. 91–99.
- [7] Z. Zhuang, M. Tan, B. Zhuang, J. Liu, Y. Guo, Q. Wu, J. Huang, and J. Zhu, "Discrimination-aware channel pruning for deep neural networks," in *Proc. Adv. Neural Inf. Process. Syst.*, 2018, pp. 883–894.
- [8] Y. He, X. Zhang, and J. Sun, "Channel pruning for accelerating very deep neural networks," in *Proc. IEEE Int. Conf. Comp. Vis.*, vol. 2, 2017, p. 6.
- [9] S. Lin, R. Ji, C. Yan, B. Zhang, L. Cao, Q. Ye, F. Huang, and D. Doermann, "Towards optimal structured cnn pruning via generative adversarial learning," in *Proc. IEEE Conf. Comp. Vis. Patt. Recogn.*, 2019, pp. 2790–2799.
- [10] B. Zhuang, C. Shen, M. Tan, L. Liu, and I. Reid, "Towards effective low-bitwidth convolutional neural networks," in *Proc. IEEE Conf. Comp. Vis. Patt. Recogn.*, 2018, pp. 7920–7928.
- [11] B. Jacob, S. Kligys, B. Chen, M. Zhu, M. Tang, A. Howard, H. Adam, and D. Kalenichenko, "Quantization and training of neural networks for efficient integer-arithmetic-only inference," in *Proc. IEEE Conf. Comp. Vis. Patt. Recogn.*, 2018, pp. 2704–2713.
- [12] F. Chollet, "Xception: Deep learning with depthwise separable convolutions," in *Proc. IEEE Conf. Comp. Vis. Patt. Recogn.*, 2017, pp. 1251–1258.
- [13] A. G. Howard, M. Zhu, B. Chen, D. Kalenichenko, W. Wang, T. Weyand, M. Andreetto, and H. Adam, "Mobilenets: Efficient convolutional neural networks for mobile vision applications," *arXiv preprint arXiv:1704.04861*, 2017.
- [14] A. Ehliar, "Area efficient floating-point adder and multiplier with ieee-754 compatible semantics," in *Field-Programmable Technology (FPT), 2014 International Conference on*. IEEE, pp. 131–138.
- [15] G. Govindu, L. Zhuo, S. Choi, and V. Prasanna, "Analysis of high-performance floating-point arithmetic on fpgas," in *Parallel and Distributed Processing Symposium, 2004. Proceedings. 18th International*. IEEE, 2004, p. 149.
- [16] I. Hubara, M. Courbariaux, D. Soudry, R. El-Yaniv, and Y. Bengio, "Binarized neural networks," in *Proc. Adv. Neural Inf. Process. Syst.*, 2016, pp. 4107–4115.
- [17] M. Rastegari, V. Ordonez, J. Redmon, and A. Farhadi, "Xnor-net: Imagenet classification using binary convolutional neural networks," in *Proc. Eur. Conf. Comp. Vis.*, 2016, pp. 525–542.
- [18] A. Polino, R. Pascanu, and D. Alistarh, "Model compression via distillation and quantization," in *Proc. Int. Conf. Learn. Repres.*, 2018.
- [19] A. Mishra and D. Marr, "Apprentice: Using knowledge distillation techniques to improve low-precision network accuracy," in *Proc. Int. Conf. Learn. Repres.*, 2018.
- [20] L. Hou and J. T. Kwok, "Loss-aware weight quantization of deep networks," in *Proc. Int. Conf. Learn. Repres.*, 2018.
- [21] L. Hou, Q. Yao, and J. T. Kwok, "Loss-aware binarization of deep networks," in *Proc. Int. Conf. Learn. Repres.*, 2017.
- [22] S. Zhou, Y. Wu, Z. Ni, X. Zhou, H. Wen, and Y. Zou, "Dorefa-net: Training low bitwidth convolutional neural networks with low bitwidth gradients," *arXiv preprint arXiv:1606.06160*, 2016.
- [23] Z. Cai, X. He, J. Sun, and N. Vasconcelos, "Deep learning with low precision by half-wave gaussian quantization," in *Proc. IEEE Conf. Comp. Vis. Patt. Recogn.*, 2017, pp. 5918–5926.
- [24] D. Zhang, J. Yang, D. Ye, and G. Hua, "Lq-nets: Learned quantization for highly accurate and compact deep neural networks," in *Proc. Eur. Conf. Comp. Vis.*, 2018, pp. 365–382.
- [25] L.-C. Chen, G. Papandreou, I. Kokkinos, K. Murphy, and A. L. Yuille, "Deeplab: Semantic image segmentation with deep convolutional nets, atrous convolution, and fully connected crfs," *IEEE Trans. Pattern Anal. Mach. Intell.*, vol. 40, no. 4, pp. 834–848, 2018.
- [26] L.-C. Chen, G. Papandreou, F. Schroff, and H. Adam, "Rethinking atrous convolution for semantic image segmentation," *arXiv preprint arXiv:1706.05587*, 2017.
- [27] Y. Guo, A. Yao, H. Zhao, and Y. Chen, "Network sketching: Exploiting binary structure in deep cnns," in *Proc. IEEE Conf. Comp. Vis. Patt. Recogn.*, 2017, pp. 5955–5963.
- [28] Z. Li, B. Ni, W. Zhang, X. Yang, and W. Gao, "Performance guaranteed network acceleration via high-order residual quantization," in *Proc. IEEE Int. Conf. Comp. Vis.*, 2017, pp. 2584–2592.
- [29] X. Lin, C. Zhao, and W. Pan, "Towards accurate binary convolutional neural network," in *Proc. Adv. Neural Inf. Process. Syst.*, 2017, pp. 344–352.
- [30] J. Fromm, S. Patel, and M. Philipose, "Heterogeneous bitwidth bi-

narization in convolutional neural networks," in *Proc. Adv. Neural Inf. Process. Syst.*, 2018, pp. 4006–4015.

[31] W. Tang, G. Hua, and L. Wang, "How to train a compact binary neural network with high accuracy?" in *Proc. AAAI Conf. on Arti. Intel.*, 2017, pp. 2625–2631.

[32] F. N. Iandola, S. Han, M. W. Moskewicz, K. Ashraf, W. J. Dally, and K. Keutzer, "SqueezeNet: Alexnet-level accuracy with 50x fewer parameters and; 0.5 mb model size," *arXiv preprint arXiv:1602.07360*, 2016.

[33] X. Zhang, X. Zhou, M. Lin, and J. Sun, "Shufflenet: An extremely efficient convolutional neural network for mobile devices," in *Proc. IEEE Conf. Comp. Vis. Patt. Recogn.*, 2018, pp. 6848–6856.

[34] B. Zoph and Q. V. Le, "Neural architecture search with reinforcement learning," in *Proc. Int. Conf. Learn. Repren.*, 2017.

[35] H. Pham, M. Y. Guan, B. Zoph, Q. V. Le, and J. Dean, "Efficient neural architecture search via parameter sharing," in *Proc. Int. Conf. Mach. Learn.*, 2018, pp. 4092–4101.

[36] B. Zoph, V. Vasudevan, J. Shlens, and Q. V. Le, "Learning transferable architectures for scalable image recognition," in *Proc. IEEE Conf. Comp. Vis. Patt. Recogn.*, 2018, pp. 8697–8710.

[37] B. Zhuang, C. Shen, M. Tan, L. Liu, and I. Reid, "Structured binary neural network for accurate image classification and semantic segmentation," in *Proc. IEEE Conf. Comp. Vis. Patt. Recogn.*, 2019, pp. 413–422.

[38] F. Li, B. Zhang, and B. Liu, "Ternary weight networks," *arXiv preprint arXiv:1605.04711*, 2016.

[39] C. Zhu, S. Han, H. Mao, and W. J. Dally, "Trained ternary quantization," *Proc. Int. Conf. Learn. Repren.*, 2017.

[40] J. Choi, Z. Wang, S. Venkataramani, P. I.-J. Chuang, V. Srinivasan, and K. Gopalakrishnan, "Pact: Parameterized clipping activation for quantized neural networks," *arXiv preprint arXiv:1805.06085*, 2018.

[41] S. Jung, C. Son, S. Lee, J. Son, J.-J. Han, Y. Kwak, S. J. Hwang, and C. Choi, "Learning to quantize deep networks by optimizing quantization intervals with task loss," in *Proc. IEEE Conf. Comp. Vis. Patt. Recogn.*, 2019, pp. 4350–4359.

[42] E. Park, J. Ahn, and S. Yoo, "Weighted-entropy-based quantization for deep neural networks," in *Proc. IEEE Conf. Comp. Vis. Patt. Recogn.*, 2017, pp. 5456–5464.

[43] R. Ding, T.-W. Chin, Z. Liu, and D. Marculescu, "Regularizing activation distribution for training binarized deep networks," in *Proc. IEEE Conf. Comp. Vis. Patt. Recogn.*, 2019, pp. 11 408–11 417.

[44] Y. Bai, Y.-X. Wang, and E. Liberty, "Proxquant: Quantized neural networks via proximal operators," in *Proc. Int. Conf. Learn. Repren.*, 2019.

[45] K. Wang, Z. Liu, Y. Lin, J. Lin, and S. Han, "Haq: Hardware-aware automated quantization with mixed precision," in *Proc. IEEE Conf. Comp. Vis. Patt. Recogn.*, 2019, pp. 8612–8620.

[46] C. Szegedy, W. Liu, Y. Jia, P. Sermanet, S. Reed, D. Anguelov, D. Erhan, V. Vanhoucke, and A. Rabinovich, "Going deeper with convolutions," in *Proc. IEEE Conf. Comp. Vis. Patt. Recogn.*, 2015, pp. 1–9.

[47] C. Szegedy, V. Vanhoucke, S. Ioffe, J. Shlens, and Z. Wojna, "Rethinking the inception architecture for computer vision," in *Proc. IEEE Conf. Comp. Vis. Patt. Recogn.*, 2016, pp. 2818–2826.

[48] C. Szegedy, S. Ioffe, V. Vanhoucke, and A. A. Alemi, "Inception-v4, inception-resnet and the impact of residual connections on learning," in *Proc. AAAI Conf. on Arti. Intel.*, vol. 4, 2017, p. 12.

[49] M. Sandler, A. Howard, M. Zhu, A. Zhmoginov, and L.-C. Chen, "Mobilenetv2: Inverted residuals and linear bottlenecks," in *Proc. IEEE Conf. Comp. Vis. Patt. Recogn.*, 2018, pp. 4510–4520.

[50] C. Liu, B. Zoph, J. Shlens, W. Hua, L.-J. Li, L. Fei-Fei, A. Yuille, J. Huang, and K. Murphy, "Progressive neural architecture search," in *Proc. Eur. Conf. Comp. Vis.*, 2018, pp. 19–34.

[51] H. Liu, K. Simonyan, O. Vinyals, C. Fernando, and K. Kavukcuoglu, "Hierarchical representations for efficient architecture search," in *Proc. Int. Conf. Learn. Repren.*, 2018.

[52] Z. Zhang, X. Zhang, C. Peng, X. Xue, and J. Sun, "Exfuse: Enhancing feature fusion for semantic segmentation," in *Proc. Eur. Conf. Comp. Vis.*, 2018, pp. 269–284.

[53] S. Mehta, M. Rastegari, A. Caspi, L. Shapiro, and H. Hajishirzi, "EspNet: Efficient spatial pyramid of dilated convolutions for semantic segmentation," in *Proc. Eur. Conf. Comp. Vis.*, 2018, pp. 552–568.

[54] G. Lin, A. Milan, C. Shen, and I. Reid, "Refinenet: Multi-path refinement networks for high-resolution semantic segmentation," in *Proc. IEEE Conf. Comp. Vis. Patt. Recogn.*, 2017, pp. 1925–1934.

[55] G. Lin, C. Shen, A. Van Den Hengel, and I. Reid, "Efficient piecewise training of deep structured models for semantic segmentation," in *Proc. IEEE Conf. Comp. Vis. Patt. Recogn.*, 2016, pp. 3194–3203.

[56] S. Chandra and I. Kokkinos, "Fast, exact and multi-scale inference for semantic image segmentation with deep gaussian crfs," in *Proc. Eur. Conf. Comp. Vis.*, 2016, pp. 402–418.

[57] C. Liu, L.-C. Chen, F. Schroff, H. Adam, W. Hua, A. Yuille, and L. Fei-Fei, "Auto-deeplab: Hierarchical neural architecture search for semantic image segmentation," in *Proc. IEEE Conf. Comp. Vis. Patt. Recogn.*, 2019, pp. 82–92.

[58] V. Nekrasov, H. Chen, C. Shen, and I. Reid, "Fast neural architecture search of compact semantic segmentation models via auxiliary cells," in *Proc. IEEE Conf. Comp. Vis. Patt. Recogn.*, 2019, pp. 9126–9135.

[59] C. Yu, J. Wang, C. Peng, C. Gao, G. Yu, and N. Sang, "Bisenet: Bilateral segmentation network for real-time semantic segmentation," in *Proc. Eur. Conf. Comp. Vis.*, 2018, pp. 325–341.

[60] S. Mehta, M. Rastegari, L. Shapiro, and H. Hajishirzi, "EspNetv2: A light-weight, power efficient, and general purpose convolutional neural network," *arXiv preprint arXiv:1811.11431*, 2018.

[61] R. Girshick, "Fast r-cnn," in *Proc. IEEE Int. Conf. Comp. Vis.*, 2015, pp. 1440–1448.

[62] R. Girshick, J. Donahue, T. Darrell, and J. Malik, "Rich feature hierarchies for accurate object detection and semantic segmentation," in *Proc. IEEE Conf. Comp. Vis. Patt. Recogn.*, 2014, pp. 580–587.

[63] J. Redmon and A. Farhadi, "Yolo9000: better, faster, stronger," in *Proc. IEEE Conf. Comp. Vis. Patt. Recogn.*, 2017, pp. 7263–7271.

[64] —, "Yolov3: An incremental improvement," *arXiv preprint arXiv:1804.02767*, 2018.

[65] W. Liu, D. Anguelov, D. Erhan, C. Szegedy, S. Reed, C.-Y. Fu, and A. C. Berg, "Ssd: Single shot multibox detector," in *Proc. Eur. Conf. Comp. Vis.*, 2016, pp. 21–37.

[66] T.-Y. Lin, P. Goyal, R. Girshick, K. He, and P. Dollár, "Focal loss for dense object detection," in *Proc. IEEE Int. Conf. Comp. Vis.*, 2017, pp. 2980–2988.

[67] G. Chen, W. Choi, X. Yu, T. Han, and M. Chandraker, "Learning efficient object detection models with knowledge distillation," in *Proc. Adv. Neural Inf. Process. Syst.*, 2017, pp. 742–751.

[68] Y. Wei, X. Pan, H. Qin, W. Ouyang, and J. Yan, "Quantization mimic: Towards very tiny cnn for object detection," in *Proc. Eur. Conf. Comp. Vis.*, 2018, pp. 267–283.

[69] M. Tan, B. Chen, R. Pang, V. Vasudevan, M. Sandler, A. Howard, and Q. V. Le, "Mnasnet: Platform-aware neural architecture search for mobile," in *Proc. IEEE Conf. Comp. Vis. Patt. Recogn.*, 2019, pp. 2820–2828.

[70] Z. Tian, C. Shen, H. Chen, and T. He, "Fcos: Fully convolutional one-stage object detection," in *Proc. IEEE Int. Conf. Comp. Vis.*, 2019.

[71] W. Liu, S. Liao, W. Ren, W. Hu, and Y. Yu, "High-level semantic feature detection: A new perspective for pedestrian detection," in *Proc. IEEE Conf. Comp. Vis. Patt. Recogn.*, 2019, pp. 5187–5196.

[72] Y. Bengio, N. Léonard, and A. Courville, "Estimating or propagating gradients through stochastic neurons for conditional computation," *arXiv preprint arXiv:1308.3432*, 2013.

[73] Z. Liu, B. Wu, W. Luo, X. Yang, W. Liu, and K.-T. Cheng, "Bi-real net: Enhancing the performance of 1-bit cnns with improved representational capability and advanced training algorithm," in *Proc. Eur. Conf. Comp. Vis.*, 2018, pp. 722–737.

[74] T.-Y. Lin, P. Dollár, R. Girshick, K. He, B. Hariharan, and S. Belongie, "Feature pyramid networks for object detection," in *Proc. IEEE Conf. Comp. Vis. Patt. Recogn.*, 2017, pp. 2117–2125.

[75] M. Courbariaux, Y. Bengio, and J.-P. David, "Binaryconnect: Training deep neural networks with binary weights during propagations," in *Proc. Adv. Neural Inf. Process. Syst.*, 2015, pp. 3123–3131.

[76] A. Zhou, A. Yao, Y. Guo, L. Xu, and Y. Chen, "Incremental network quantization: Towards lossless cnns with low-precision weights," *Proc. Int. Conf. Learn. Repren.*, 2017.

[77] S. Xie, R. Girshick, P. Dollár, Z. Tu, and K. He, "Aggregated residual transformations for deep neural networks," in *Proc. IEEE Conf. Comp. Vis. Patt. Recogn.*, 2017, pp. 5987–5995.

[78] H. Liu, K. Simonyan, and Y. Yang, "Darts: Differentiable architecture search," in *Proc. Int. Conf. Learn. Repren.*, 2019.

[79] M. Tan and Q. V. Le, "Efficientnet: Rethinking model scaling for convolutional neural networks," in *Proc. Int. Conf. Mach. Learn.*, 2019, pp. 6105–6114.

- [80] Z. Liu, W. Luo, B. Wu, X. Yang, W. Liu, and K.-T. Cheng, "Bi-real net: Binarizing deep network towards real-network performance," *arXiv preprint arXiv:1811.01335*, 2018.
- [81] J. Bethge, M. Bornstein, A. Loy, H. Yang, and C. Meinel, "Training competitive binary neural networks from scratch," *arXiv preprint arXiv:1812.01965*, 2018.
- [82] O. Russakovsky, J. Deng, H. Su, J. Krause, S. Satheesh, S. Ma, Z. Huang, A. Karpathy, A. Khosla, M. Bernstein *et al.*, "Imagenet large scale visual recognition challenge," *Int. J. Comp. Vis.*, vol. 115, no. 3, pp. 211–252, 2015.
- [83] D. P. Kingma and J. Ba, "Adam: A method for stochastic optimization," in *Proc. Int. Conf. Learn. Repren.*, 2015.
- [84] A. Paszke, S. Gross, S. Chintala, G. Chanan, E. Yang, Z. DeVito, Z. Lin, A. Desmaison, L. Antiga, and A. Lerer, "Automatic differentiation in pytorch," in *Proc. Adv. Neural Inf. Process. Syst. Workshops*, 2017.
- [85] J. Bethge, H. Yang, C. Bartz, and C. Meinel, "Learning to train a binary neural network," *arXiv preprint arXiv:1809.10463*, 2018.
- [86] J. Faraone, N. Fraser, M. Blott, and P. H. Leong, "Syq: Learning symmetric quantization for efficient deep neural networks," in *Proc. IEEE Conf. Comp. Vis. Patt. Recogn.*, 2018, pp. 4300–4309.
- [87] M. Everingham, L. Van Gool, C. K. Williams, J. Winn, and A. Zisserman, "The pascal visual object classes (voc) challenge," *Int. J. Comp. Vis.*, vol. 88, no. 2, pp. 303–338, 2010.
- [88] B. Hariharan, P. Arbeláez, L. Bourdev, S. Maji, and J. Malik, "Semantic contours from inverse detectors," in *Proc. IEEE Int. Conf. Comp. Vis.*, 2011, pp. 991–998.
- [89] T.-Y. Lin, M. Maire, S. Belongie, J. Hays, P. Perona, D. Ramanan, P. Dollár, and C. L. Zitnick, "Microsoft coco: Common objects in context," in *Proc. Eur. Conf. Comp. Vis.*, 2014, pp. 740–755.
- [90] C. Baskin, E. Schwartz, E. Zheltonozhskii, N. Liss, R. Giryes, A. M. Bronstein, and A. Mendelson, "Uniq: Uniform noise injection for non-uniform quantization of neural networks," *arXiv preprint arXiv:1804.10969*, 2018.